Both $P_c$ and $P_t$ are expected to be dependent upon the projection of the length of the vehicle on the direction of the electric field gradient. Because the Galileo Probe is substantially smaller than the aircraft considered, it might appear that the estimates of $P_c$ and $P_t$ should be reduced. However, the parachute attached to the Galileo Probe on its descent must be considered. If the parachute or its attachment cords become coated with aerosols or droplets during the passage through the clouds, the vehicle will intensify the field much more than if the probe descended alone. It will be assumed that the parachute and its attachment cords will be sufficiently conductive to cause field intensification. The length of the probe and parachute is 15 m. Consequently, the Galileo Probe with its parachute will intensify the vertical electric fields about as much as a commercial aircraft and somewhat more than an F-106B. The assumption that the intensification of the field by the probe is the same as that due to a commercial aircrat will tend to overestimate $P_c$ because the horizontal field intensification will be smaller than that caused by the aircraft. However, because $P_c = 3 \times 10^{-4}$ probably underestimates the results of the commercial airline experience, the two factors will tend to compensate. Similarly, the larger vertical, but smaller horizontal, extent of the probe relative to the F-106B will tend to compensate. Therefore, "ball park" estimates of $P_c$ and $P_t$ will be obtained by setting them equal to those for aircraft flying through terrestrial clouds.

Next $P_s$ will be calculated from $P_c$ and $P_t$, and the fraction, $f$, of Jupiter covered by thunderstorms. An examination of the Voyager I images of the dark side of Jupiter shows that approximately 0.2% of the surface is covered with lightning flashes. Because the Voyager camera could detect only the brightest flashes, the total area covered by thunderstorms could be significantly larger.[1] $P_s$ can now be estimated from

$$P_s = f * P_t + (1-f) * P_c * T = 0.002 * 0.42 + 0.998 * 3 \times 10^{-4} * 1 = 0.001 \quad (1)$$

where $T$ is the flight time through the clouds. Although the duration of the flight between the top of the ammonia clouds and the base of the water clouds is expected to be near 1 h,[10] $T$ could be somewhat less than 1 h if there are clear gaps between the cloud layers.

It is important to recognize the substantial uncertainties involved in each of the steps. The uncertainties arise from our lack of knowledge of the magnitude and extent of electric fields in the Jovian clouds as well as the lack of a validated theory that relates the strike probability to the magnitude of the electric field and the field intensification factor. Although an effort can be made to remedy the latter problem, no measurements of the electric fields in the clouds of Jupiter are available. No electric field measurements will be made by the Galileo probe, and no further missions to Jupiter are planned this century. Hence, a determination of the uncertainty in $P_s$ appears unlikely in the near future. Consequently, $P_s$ should be regarded as a "ball park" estimate with a large uncertainty.

Although the estimate of a strike to the probe is only 0.001, it is about the same as the expected failure rate due to other design factors. Therefore, when entry probes to cloud-covered planets are designed, it seems appropriate to consider measures to protect the vehicle and its payload from lightning activity.

## References

[1]Borucki, W.J., Bar-Nun, A., Scarf, F.L., Cook, A.F., II, and Hunt, G.E., "Lightning Activity on Jupiter," *Icarus,* Vol. 52, Dec. 1982, pp. 492-502.

[2]Fisher F.A. and Plumer, J.A., "Lightning Protection of Aircraft," NASA RP-1008, 1977.

[3]Hacker, P.T., "Lightning Damage to a General Aviation Aircraft—Description and Analysis," NASA TN D-7775, 1974.

[4]Colin, L., "The Pioneer Venus Program," *Journal of Geophysical Research,* Vol. 85, Dec. 1980, pp. 7575-7598.

[5]Mazur, V., Fisher, B.D., and Gerlach, J.C., "Conditions Conducive to Lightning Striking on Aircraft in a Thunderstorm," *Proceedings of the Eighth International Aerospace and Ground Conference on Lightning and Static Electricity,* Fort Worth,, Texas, June 1983, pp. 90.1-90.7.

[6]Godfrey, R., Mathews, E.R., and McDivitt, J.A., Marshall Space Flight Center, Analysis of Apollo 12 Lightning Incident, MSC-01540, Feb. 1970.

[7]Fisher, B.D. and Plumer, J.A., "Lightning Attachment Patterns and Flight Conditions Experienced by the NASA F-106B Airplane," *Proceedings of the Eighth International Aerospace and Ground Conference on Lightning and Static Electricity,* Fort Worth, Texas, June 1983, p. 26.1.

[8]Krider, E.P., Noggle, R.C., Uman, M.A., and Orville, R.E., "Lightning and the Apollo 17/Saturn V Exhaust Plume," *Journal of Spacecraft and Rockets,* Vol. 11, Feb. 1974, pp. 72-75.

[9]Brook, M., Holmes, C.R., and Moore, C.B., "Lightning and Rockets: Some Implications of the Apollo 12 Lightning Event," *Naval Research Reviews,* Vol. 23, April 1970, pp. 1-17.

[10]Vojvodich, N.S., Drean, R.J., Schaupp, R.W., and Farless, D.L., "Galileo Atmospheric Entry Probe Mission Description," AIAA Paper 83-0100, Jan. 1983.

# Effects of an S-Inlet on the Flow in a Dump Combustor

J.A. Schetz,* J. Guruswamy,† and J.F. Marchman III‡
*Virginia Polytechnic Institute and State University*
*Blacksburg, Virginia*

## Introduction

THE design of a combustion chamber involves various studies, of which flowfield analysis is an important part. Some design work is done analytically using computer codes, and detailed testing is done at a later stage. There are complex configurations where a design cannot be accomplished using the available codes. Experiments with either the actual or simulated flow are a reliable means of refining design. The flow in the combustion system can often be studied as an isolated process without heat release. Previous investigations [Ref. (1)] have shown that in certain systems, e.g., the flame holder, the hot (actual) and cold (simulated) flow patterns agree closely.

Swirl is used in some combustion chambers to achieve flame stabilization and improve fuel burning. Swirl can be achieved by: 1) tangential entry of fluid, 2) rotating vanes, or 3) guide vanes. Swirl generation by vanes is most attractive for application in ramjets [Ref. (2)]. That method of swirl was used here.

The different components of the system can have a significant effect on the flow pattern in the burner. Here, the changes in flow pattern that occur due to an S-inlet instead of a straight inlet are studied. They are employed in situations where a conventional straight inlet cannot be used, such as in certerline engine jet aircraft and in cruise missiles. It is conjectured that a nonuniform flow distribution and separation may result when an S-inlet is used.

Received Sept. 29, 1983; revision received Jan. 3, 1984. 

*Professor and Department Head. Associate Fellow AIAA.
†Graduate Assistant. Student Member AIAA.
‡Associate Professor. Associate Fellow AIAA.

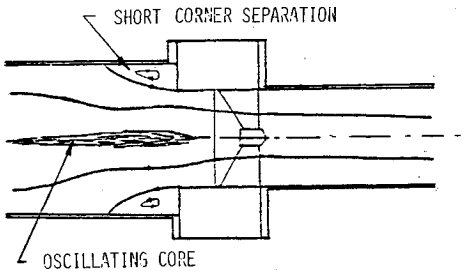


**Fig. 1a Flow pattern sketched from visual observations. Straight inlet with swirl.**

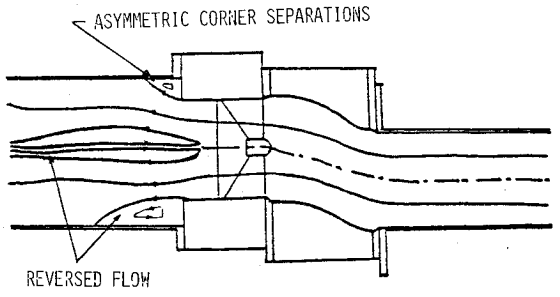


**Fig. 1b Flow pattern sketched from visual observations. S-inlet with swirl.**

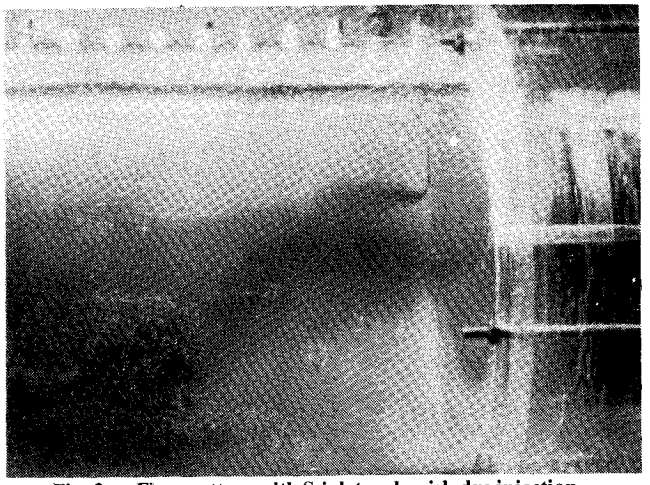

**Fig. 2a Flow pattern with S-inlet and swirl, dye injection.**

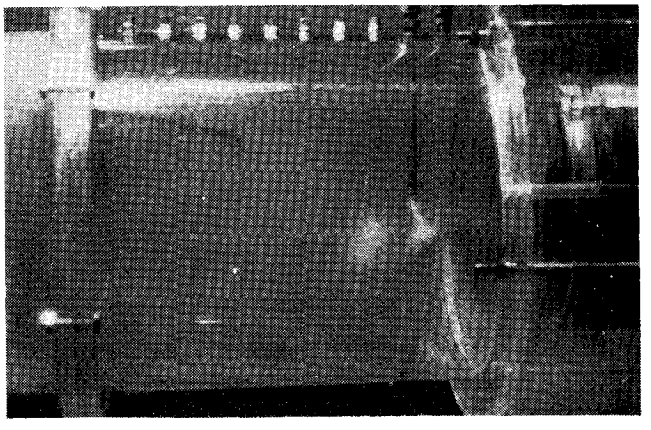

**Fig. 2b Flow pattern with S-inlet and swirl, Pliolite bead injection.**

**Legend, Figs. 3a and 3b**

| Symbol | Inlet | Swirl | Traverse |
|---|---|---|---|
| Y | Straight | No | 0 (vertical top) |
| | Straight | Yes | 0 |
| X | S | No | 0 |
| ⊠ | S | No | 180 |
| ✱ | S | No | 270 |
| ⋈ | S | Yes | 0 |
| ⋈ | S | Yes | 90 |
| ⋈ | S | Yes | 180 |
| ◈ | S | Yes | 270 |

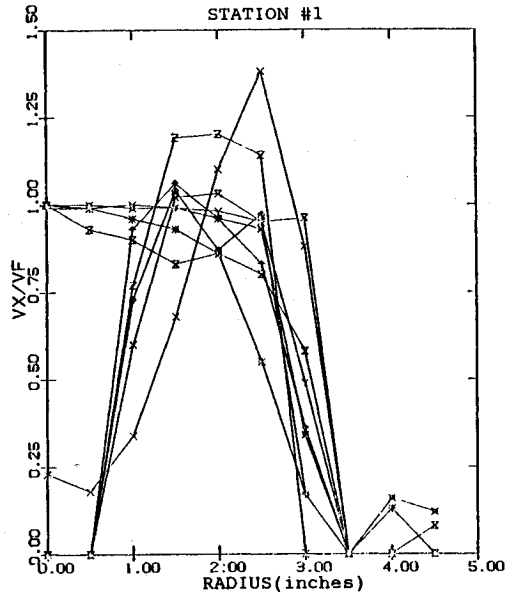


**Fig. 3a $V_x/V_f$ vs distance from centerline at $X=0.5$ in.**

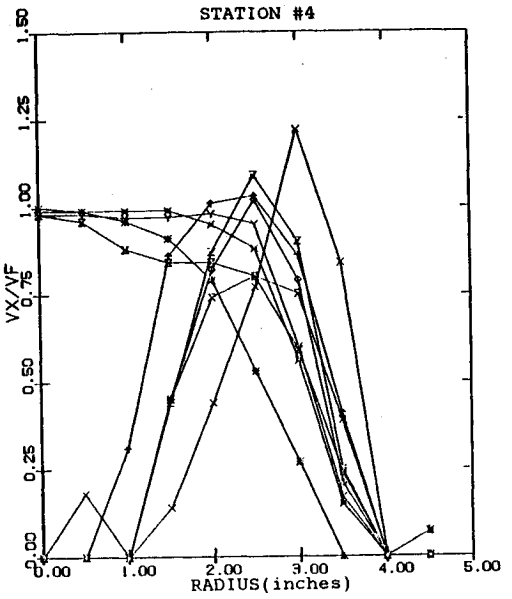


**Fig. 3b $V_x/V_f$ vs distance from centerline at $X=3.5$ in.**

**Lengend, Figs. 4 and 5.**

| Symbol | Inlet | Swirl | Traverse |
|---|---|---|---|
| Y | Straight | No | 0 (vertical top) |
| | Straight | Yes | 0 |
| X | S | No | 0 |
| ⊠ | S | No | 180 |
| ✱ | S | No | 270 |
| ⋈ | S | Yes | 0 |
| ⋈ | S | Yes | 90 |
| ✦ | S | Yes | 180 |
| ◈ | S | Yes | 270 |

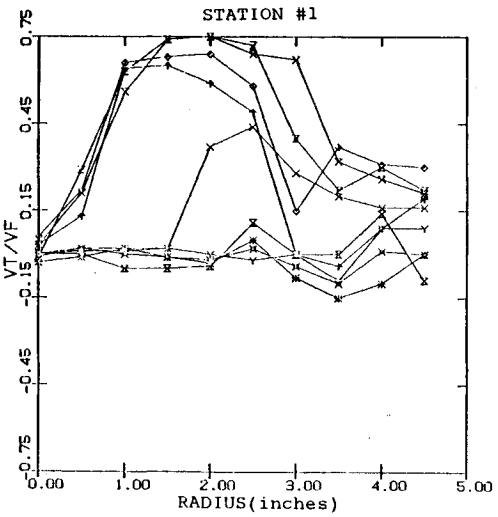


Fig. 4a $V_t/V_f$ vs distance from centerline at $X=0.5$ in.

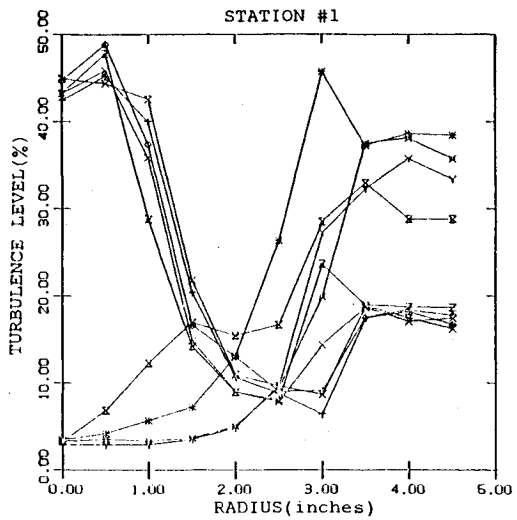


Fig. 5a Turbulence level in % vs distance from centerline at $X=0.5$ in.

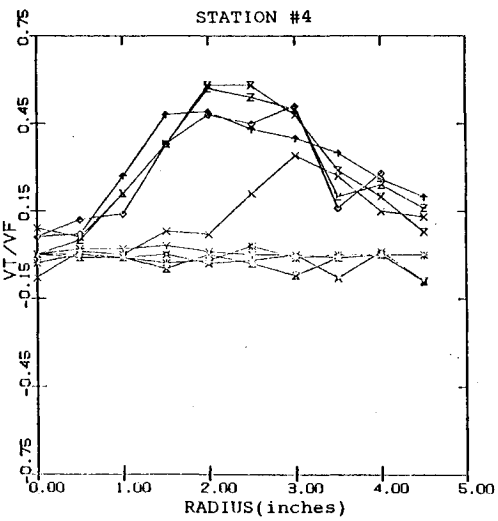


Fig. 4b $V_t/V_f$ vs distance from centerline at $X=3.5$ in.

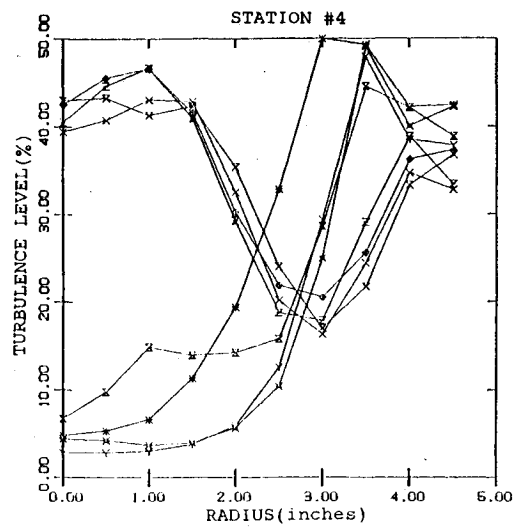


Fig. 5b Turbulence level in % vs distance fom centerline at $X=3.5$ in.

## Experimental Setup and Test Procedure

The combustion chamber, 9.5 in. in diameter and 10.5 in. long, was made of ¼ in. Plexiglas pipe. A contoured nozzle was fitted to the end of the combustion chamber. The swirler section is 6 in. in diameter and 6 in. long. The swirler had twelve vanes with varying widths out from the root. The S-inlet had a 6.5 in. diameter and a 2.0 in. centerline offset.

Tap water from a tank was pumped to the test section via an orifice plate and a filter. The water enters the entry chamber (6 in. inner diameter, 17 in. long) through two 2-in. pipes on opposite sides. This chamber was fixed to the inlet duct of the model with a wire mesh in between.

Pliolite beads (102% water density) were found to follow the streamlines of flow closely. Food coloring was also used. The water tests were at a Reynolds number of 1.0 to $4.8\times10^4$.

The model was later placed in a rectangular box into which cold air was blown via a square-edge orifice, a diffuser, and a flow straightener for testing with air.

Mean velocity measurements were made using a five-hole Pitot probe, and turbulence level measurements were made using a hot wire. All air tests were at a Reynolds number of $7.1\times10^5$.

## Results and Discussion

Some flow visualization results are shown as sketches in Figs. 1a and 1b from observations made by eye. The tests were made with the straight inlet configuration without swirl and formed the baseline case. Recirculation occurred at the corners, and the length of the recirculation zone increased with mean flow velocity. With the S-inlet, the length of the corner recirculation zone is greater at the bottom than at the top.

The size of the corner recirculation zone is considerably reduced with swirl. When the flow Reynolds number was increased to over about $10^4$, a central recirculation zone was seen behind the hub of the swirler. With the straight inlet, the central recirculation zone took the form of an oscillating core.

With the S-inlet, the swirl created a prominent central recirculation zone and an uneven corner recirculation zone. (See Figs. 2a and 2b). In Fig. 2a, the liquid dye is drawn into the low-pressure central region from downstream.

Velocity and turbulence measurements were made for traverses at seven stations in the burner. Each plot consists of nine sets of data points. Typical plots of axial velocity vs radius at two of the seven stations are shown in Figs. 3a and 3b. The points marked at $V_x/V_f=0$ are located in the recirculation zones where the $V_x/V_f$ is either zero or negative. For the nonswirling flow, $V_x/V_f$ is close to 1.0 in the center of the burner. There is a marked change in the velocity distribution at a radius of 3 in., and negative axial velocities are found to occur at greater radii. This is due to the recirculation zone formed near the wall of the burner near the exit of the swirler. The low velocity at the center for flows with swirling occurs due to the toroidal recirculation zone. The peak velocity occurs in the region between radii of 2.5 and 4 in., and the peak is well defined for the straight inlet configuration. The difference in velocity profiles for the four directions of traverse in the S-inlet configuration with swirling flow shows the absence of symmetry in the streamlines in the combustion chamber. Two notable aspects of the flow with the S-inlet when compared with that for the straight inlet are the more pronounced central recirculation zone and the occurrence of unequal corner recirculation zones.

Typical tangential velocity profiles are shown in Figs. 4a and 4b. The tangential velocity is close to zero near the axis of the burner for the nonswirling flow. This component is smaller in the straight duct for swirling flows. $V_t/V_f$ is close to zero to a radius of 1.5 in. in the straight configuration, but increases with radius for the S-inlet configuration.

Some plots of turbulence level vs radius are shown in Figs. 5a and 5b. The level in the nonswirling flow is higher with the S-inlet near the center of the chamber. At the top, the variation is different from the sides and bottom. The level is higher in the central region and lower near the wall than for the other two cases. In the region between radii of 2.0 and 4.0 in., it is found that the turbulence level of the fluid coming out of the bottom portion is highest and that for the fluid coming out of the top is lowest.

Swirling introduced a marked change in the turbulence level distribution. Close to the axis, the level was first high, then fell rapidly, and then increased again close to the wall. The turbulence distribution along the four traverse directions is more uniform for the swirling than for the nonswirling flow. Close to the exit of the swirler section, turbulence levels are essentially the same for all traverses.

The turbulence level near the wall is similar for the swirling and the nonswirling flows downstream of Station 4. Very high turbulence levels occur in the central and corner recirculation regions.

## Acknowledgment

This work was supported by Atlantic Research Corp. with Mr. Frederick Rodgers as Technical Monitor.

## References

[1]Winter, E.F., "Flow Visualization Techniques applied to Combustion Problems," *Journal of the Royal Aeronautical Society*, Vol. 62, April 1975, pp. 268-276.

[2]Buckley, P.L., Craig, R.R., Davis, D.L., and Schwartzkoff, K.G., "The Design and Combustion Performance of Practical Swirlers for Integral Rocket/Ramjets," AIAA Paper 80-1119, July 1980.